

1 Article

2

3

4

**A one-step protocol to generate impermeable fluorescent
HaloTag substrates for *in situ* live cell application and super-resolution
imaging**

5

6

7

8

9

10 Kilian Roßmann¹, Siqi Sun¹, Christina Holmboe Olesen¹, Maria Kowald¹, Eleni Tapp¹, Ulrich
11 Pabst¹, Marie Bieck¹, Ramona Birke¹, Brenda C. Shields³, PyeongHwa Jeong⁴, Jiyong
12 Hong⁴, Michael R. Tadross³, Joshua Levitz², Martin Lehmann¹, Noa Lipstein¹ and Johannes
13 Broichhagen^{1,*}

14

15 ¹ Leibniz-Forschungsinstitut für Molekulare Pharmakologie (FMP), 13125 Berlin, Germany.

16 ² Weill Cornell Medicine, Department of Biochemistry, NY, USA.

17 ³ Duke University, Department of Biomedical Engineering, Durham, North Carolina 27708,
18 USA

19 ⁴ Duke University, Department of Chemistry, Durham, North Carolina 27708, USA

20

21 * Correspondence should be addressed to:

22 broichhagen@fmp-berlin.de

23

24 **KEYWORDS:** HaloTag, fluorescence microscopy; mGluR2; impermeability; STED; ATTO
25 647N

26

27 **ORCIDs**

28

29 Kilian Roßmann: 0000-0003-4965-9669

30 Siqi Sun: 0009-0002-8291-3358

31 Christina Holmboe Olesen: 0000-0002-0575-1597

32 Maria Kowald: 0009-0001-4769-4834

33 Eleni Tapp: 0009-0005-6277-7813

34 Ulrich Pabst: 0009-0007-0529-0720

35 Marie Bieck: n/a

36 Ramona Birke: n/a

37 Brenda C. Shields: 0000-0001-9036-2686

38 PyeongHwa Jeong: 0009-0000-3796-7627

39 Jiyong Hong: 0000-0002-5253-0949

40 Michael R. Tadross: 0000-0002-7752-6380

41 Joshua Levitz: 0000-0002-8169-6323

42 Martin Lehmann: 0000-0002-8370-6353

43 Noa Lipstein: 0000-0002-0755-5899

44 Johannes Broichhagen: 0000-0003-3084-6595

45

46

47 **ABSTRACT**

48 Communication between cells is largely orchestrated by proteins on the cell surface, which
49 allow information transfer across the cell membrane. Super-resolution and single-molecule
50 visualization of these proteins can be achieved by genetically grafting HTP (HaloTag Protein)
51 into the protein of interest followed by brief incubation of cells with a dye-HTL (dye-linked
52 HaloTag Ligand). This approach allows for use of cutting-edge fluorophores optimized for
53 specific optical techniques or a cell-impermeable dye-HTL to selectively label surface proteins
54 without labeling intracellular copies. However, these two goals often conflict, as many high-
55 performing dyes exhibit membrane permeability. Traditional methods to eliminate cell
56 permeability face synthetic bottlenecks and risk altering photophysical properties. Here we
57 report that dye-HTL reagents can be made cell-impermeable by inserting a charged sulfonate
58 directly into the HTL, leaving the dye moiety unperturbed. This simple, one-step method
59 requires no purification and is compatible with both the original HTL and second-generation
60 HTL.2, the latter offering accelerated labeling. We validate such compounds, termed dye-
61 SHTL ('dye shuttle') conjugates, in live cells via widefield microscopy, demonstrating exclusive
62 membrane staining of extracellular HTP fusion proteins. In transduced primary hippocampal
63 neurons, we label mGluR2, a neuromodulatory G protein-coupled receptor (GPCR), with dyes
64 optimized for stimulated emission by depletion (STED) super-resolution microscopy, allowing
65 unprecedented accuracy in distinguishing surface and receptors from those in internal
66 compartments of the presynaptic terminal, important in neural communication. This approach
67 offers broad utility for surface-specific protein labelling.

68 INTRODUCTION

69 Self-labelling protein tags, e.g. SNAP and HTP, are at the forefront of approaches to label
70 proteins of interest bio-orthogonally with chemical moieties in living cells and tissue.¹⁻³ The
71 main application is for fluorescence microscopy, where dyes are covalently attached to HTP
72 fusion proteins to investigate protein localization and dynamics.^{4,5} A particularly important
73 superfamily of signalling proteins are cell surface receptors, which mediate information
74 transmission between cells. However, standard protocols label both the extracellular and
75 intracellular populations, including proteins in endo/lysosomal compartments and translated
76 proteins that remain in the endoplasmic reticulum (**Fig. 1A**, left). Selective labelling of the cell-
77 surface subset can be achieved with cell-impermeable dyes. Typically, this requires that the
78 dye itself bears anionic residues, e.g. carboxylates and sulfonates (**Fig. 1A**, middle)^{6,7}.
79 However, many of the best dyes for single molecule and super-resolution microscopy⁸⁻¹¹ are
80 cell permeable, limiting their utility for selective surface labelling.

81 Traditionally, dyes are made less cell permeable by custom modification to the dye
82 itself. For instance, Jonker et al., added carboxylates on the 3-position of the azetidine of
83 JaneliaFluor635 (JF₆₃₅), yielding impermeable and fluorogenic JF_{635i} for investigating
84 endocytotic turnover⁶ (**Fig. 1A, B**), and Eiring et al. reported benefits for single-molecule
85 localization microscopy with a highly charged Cy5b¹⁰. Our own laboratories have addressed
86 this in a similar vein, by fusing a sulfonate on the same azetidine position via amide bond
87 coupling using taurine, effectively converting JF₅₄₉ and JF₆₄₆ to Sulfo549 and Sulfo646 (ref⁷),
88 respectively (**Fig. 1A**, right and **Fig. 1B**), which have been used to study kainate receptor
89 stoichiometry¹² and intracellular trafficking properties of GPCR subtypes¹³.

90 A more general and effective strategy would offer a universal solution for all dyes. For
91 instance, we recently described a modified version of the SNAP ligand in which the
92 benzylguanine (BG) leaving group carries a negative charge due to incorporation of a
93 sulfonate on the 8-position of guanine, resulting in 'SBG substrates' that are released upon
94 covalent reaction (**Fig. 1A**, right and **Fig. 1B**).¹⁴ Unfortunately, this approach is not possible
95 for the HaloTag system, since the HTL leaving group is a chloride anion that cannot be
96 chemically modified.

97 In this study, we develop a simple approach for late-stage introduction of a sulfonate
98 on the amide bond that links HTL to the dye (**Fig. 1C**). We determine the photophysical
99 properties of the subsequent modified dyes, validate their lack of membrane permeability in
100 cell lines and primary neurons, and devise a protocol to quantitatively convert commercially
101 available JaneliaFluor-HTL reagents—and potentially other dyes—to enable straightforward,
102 widespread application.

103 RESULTS

104 In this work, we aimed to introduce a sulfonate on the amide bond of available dye-HTL
105 conjugates (**Fig. 1C, D**), giving access to dye-SHTL substrates. We first used molecular
106 modelling to assess if this would be tolerated by the HTP, using AutoDock 4 engine alongside
107 the two-point attraction method for covalent docking^{15,16} on the TMR-HTL bound HTP structure
108 (PDB-ID 6Y7A)¹⁷. We found that the added C3-linker bearing the sulfonate does not sterically
109 hamper the exposed dye on the protein surface (**Fig. 1E**) (see SI and **Fig. S1-S4**). Next, we
110 synthesized two dye-SHTL substrates starting with our recently reported TMR-d12 and SiR-
111 d12 dyes, the latter of which has been shown to be an outstanding candidate for STED super-
112 resolution microscopy.¹⁸ Dissolving these dye-HTL substrates in DMF and subsequently
113 adding sodium hydride (NaH 60% in mineral oil) before 1,3 propane sultone, led to clean
114 conversion, yielding TMR-d12-SHTL and SiR-d12-SHTL within an hour in 94% and 91% yield,
115 respectively, after HPLC purification (**Fig. 1F**) (see SI). Introduction of the charged sulfonate
116 only slightly changed the excitation and emission profiles, as illustrated for TMR-d12 (HTL:
117 $\lambda_{Ex/Em} = 553/577$ nm; SHTL: $\lambda_{Ex/Em} = 554/579$ nm) (**Fig. 1G, L**). Full protein mass spectrometry
118 on recombinant HTP (ref⁷) confirmed that TMR-d12-SHTL and SiR-d12-SHTL bind to HTP
119 with quantitative stoichiometry (**Fig. 1H**), with no significant difference in labelling kinetics as
120 determined by fluorescence polarization ($t_{1/2} \sim 50$ sec) (**Fig. 1I**). We next measured quantum
121 yields (**Fig. 1J, L**) and fluorescence lifetimes (**Fig. 1K, L**) to test if sulfonation impairs dye
122 photophysics. The same trend in increasing quantum yield upon binding to HTP was observed
123 for all dyes ($\Phi_{HTP-free} = 47-49\%$; $\Phi_{HTP-bound} \sim 53\%$), while the sulfonated versions displayed up
124 to 11% longer fluorescence lifetimes over non-sulfonated precursors (**Fig. 1L**).

125 We next tested both dyes in HEK293 cells transiently transfected with our previously
126 reported SNAP-TM-HTP and HTP-TM-SNAP constructs⁷. Having each tag residing on the
127 opposite side of the cellular membrane separated by a single transmembrane (TM) domain
128 enabled us to simultaneously assess membrane permeability and labelling with built-in
129 controls for expression and cell health. We first used HTP-TM-SNAP cells, using the cell-
130 permeable BG-JF₆₄₆ to label all intracellular proteins, co-applied for 30 minutes with either
131 TMR-d12-HTL (**Fig. 2A**, upper row) or TMR-d12-SHTL (**Fig. 2A**, lower row). As expected,
132 TMR-d12-HTL showed considerable intracellular signals (**Fig. 2B**) confirmed by the similarity
133 of line-scan profiles to the BG-JF₆₄₆ intracellular reference (**Fig. 2C**, raw fluorescence left and
134 normalized right). By contrast, TMR-d12-SHTL (**Fig. 2E**) exhibited selective surface labelling,
135 with line scans differing considerably from the intracellular reference. We then swapped the
136 self-labelling tags with the SNAP-TM-HTP construct, switching to a cell-impermeable
137 BG-SulfoJF₆₄₆ so that the SNAP label serves as a surface-exclusive reference. Consistent
138 with our prior findings, TMR-d12-HTL (**Fig. 2F**, upper row) exhibited intracellular labelling (**Fig.**

139 **2G, H**), while TMR-d12-SHTL (**Fig. 2F**, lower row) showed no detectable labelling (**Fig. 2I, J**).
140 The same experiment was conducted with SiR-d12 fused to HTL (**Fig. 2K-O**) vs. SHTL (**Fig.**
141 **2P-T**) and respective red fluorophores (BG-JF₅₄₉ and BG-Sulfo549), confirming that SHTL
142 shows no membrane permeability regardless of the fluorophore. We further titrated SiR-d12
143 HTL and SHTL conjugates up to 5000 nM on HTP-TM-SNAP expressing HEK293 cells, and
144 again observed clear membrane staining for sulfonated versions (**Fig. S5**)

145 We next used lentiviral particles to transduce primary mouse hippocampal neurons
146 with a HTP-fused metabotropic glutamate receptor 2 (HTP-mGluR2) (**Fig. 3A**), which has
147 been shown to maintain identical glutamate sensitivity¹⁹ and trafficking¹³ compared to
148 untagged receptors. mGluR2 is a family C member of the G protein-coupled receptors involved
149 in modulation of synaptic transmission and serves as a potential target for the treatment of
150 neurological and psychiatric disorders²⁰. The endogenous localization of mGluR2 is along
151 axons and presynaptic sites²¹, although the precise sub-synaptic localization is not fully
152 understood.^{20,22} We aimed to determine the subcellular HTP-mGluR2 distribution by antibody
153 staining against known markers of dendritic (MAP2), presynaptic (Bassoon) and postsynaptic
154 (Shank) sites (**Fig. 3B**). One week after transduction, we applied 500 nM of SiR-d12 (-HTL or
155 -SHTL) to live cells for 30 minutes before fixation and imaging on a confocal microscope. The
156 HTL variant gave rise to pronounced signals stemming from intracellular sites in the soma
157 (**Fig. 3C**, and **Fig. S6C**), quantified by defining regions of interest around cell bodies, localized
158 by terminating dendritic MAP2 staining, and calculating the mean intensity. Non-transduced
159 neurons did not show SiR labelling (**Fig. S6A, B**), indicating that SiR-d12-HTL selectively
160 labels HTP-mGluR2 in all cellular compartments. By contrast, with SiR-d12-SHTL, the
161 fluorescent signal was significantly reduced in the soma (**Fig. 3D**), with all remaining
162 fluorescence appearing to stem from the cell surface, and in processes that were either MAP2
163 positive (**Fig. 3E**) or negative (**Fig. 3F**), revealing that a substantial intracellular population of
164 HTP-mGluR2 likely exists in all 3 sites.

165 As an important control, anti-MAP2 intensities were identical in SiR-d12-HTL and SiR-
166 d12-SHTL samples (**Fig. 3G**). Of note, MAP2 is known to locate in dendrites and not in axons,
167 and most synapses in this preparation are axo-dendritic. To identify synapses, antibodies
168 against Bassoon (presynaptic marker) and Shank (postsynaptic marker) were applied (**Fig.**
169 **3B, H**) alongside SiR-d12-SHTL. Merging the channels (**Fig. 3I**) to perform line scans revealed
170 a tendency towards pre-synaptic localization of HTP-mGluR2 with Bassoon (**Fig. 3J**), as
171 revealed by plotting pixel distances of the respective intensity maxima (**Fig. 3K**). Such
172 experiments outperform SiR-d12-HTL treated preparations (**Fig. 3L**), where signals likely
173 include receptors in intracellular sites (**Fig. 3M**), therefore rendering synaptic allocation less
174 precise, i.e. non-significant when comparing pixel distance (**Fig. 3N**, and **Fig. S6D, E**). This
175 underlines the critical impact of true surface labelling to interrogate glutamate-responsive

176 protein pools, since distances to release sites have been shown to be important for neural
177 activity²³.

178 After using confocal microscopy, we next turned to stimulated emission by depletion
179 (STED) super-resolution imaging on these samples (**Fig. 4A**), keeping in mind that SiR-d12 is
180 an excellent dye for this imaging technique¹⁸. Probing processes by a line scan revealed the
181 extracellular HTP-mGluRs with a resolution of 134 nm (**Fig. 4B**) with full width at half maxima
182 (FWHM) values of 60 and 68 nm (cf. confocal: FWHM = 259 nm). Furthermore, having a red
183 fluorophore linked antibody targeted by immunohistochemistry against Bassoon, we were able
184 to perform two-color STED on the contact site of a presynaptic site onto the process (**Fig. 4C**).
185 This demonstrated the usefulness of addressing distinct pools of proteins in combination with
186 super-resolution imaging, gaining information of neural ultrastructures.

187 ATTO 647N is a prominent dye that has been employed in STED^{24,25} and structured
188 illumination microscopy (SIM)^{26,27} super-resolution imaging, and its HTL derivative has been
189 used to stain neurons in *Drosophila*²⁸. It is characterized to be a bright dye in the far-red, which
190 is favorable. However, when examining its molecular structure, we noted a four carbon linker
191 on the 3 position for conjugation (**Fig. 5A**), which could exacerbate its intrinsic stickiness²⁹.
192 Moreover, we suspected that this linker would slow binding to HTP, given that secondary
193 interaction sites between the HTP surface and rhodamine dyes are known to underlie the rapid
194 labelling speed of dye-HTL conjugates, whereas ligands that do not bear a properly positioned
195 dye or lack a dye are known to bind HTP inefficiently³⁰. This limitation has been recently
196 overcome by the design of a second-generation HTL.2³¹, which dramatically improves the
197 efficiency of the DART (drug acutely restricted by tethering) approach³².

198 To examine whether our sulfonation approach could extend to HTL.2, we synthesized
199 ATTO 647N-HTL and ATTO 647N-HTL.2, before subjecting both to the sulfonation protocol to
200 yield ATTO 647N-SHTL and ATTO 647N-S₂HTL.2, the latter of which bears two sulfonates as
201 both amides are alkylated (**Fig. 5B**). To characterize nonspecific stickiness, we incubated non-
202 transfected HEK293 cells with 1000 nM of each compound, observing massive non-specific
203 staining for ATTO 647N-HTL (**Fig. S7B**), which was reduced for ATTO 647N-SHTL and ATTO
204 647N-HTL.2 (**Fig. S7C, D**), and lowest for ATTO 647N-S₂HTL.2 (**Fig. S7E**).

205 We confirmed that the ATTO 647-(S)HTL (**Fig. S7A**) and ATTO 647-(S₂)HTL.2 (**Fig.**
206 **5C**) cleanly react with recombinant HTP. We also investigated labelling kinetics by incubating
207 50 nM solutions of the HTL ligands with an excess of recombinant HTP (200 nM) while tracing
208 fluorescence polarization. While this did not reveal detectable differences (**Fig. 5D**), the assay
209 lacked the sensitivity needed to examine the biologically relevant case, in which low-
210 nanomolar HTL in free solution outnumbers immobilized HTP molecules. We thus turned to
211 the application of interest, using HEK293 cells encoding HTP-SNAP-mGluR2, incubated with
212 HTL ligands in a titration series (1, 10 and 100 nM) for only 10 minutes before fixation. We

213 used sparse expression with low amounts of DNA (50 ng vs. 400 ng as in Fig. 2) to ensure
214 that the labelling reaction does not deplete ligand in free solution, particularly at the low
215 concentrations. We co-labelled with the cell-impermeable BG-SulfoJF₅₄₉ (1 μ M) to visualize
216 the ideal pattern of surface-only labelling (note: HTP and SNAP are both extracellular).

217 The non-sulfonated ATTO 647N-HTL exhibited little labelling at 1 to 10 nM, while 100
218 to 1000 nM yielded predominantly nonspecific intracellular labelling that overshadowed any
219 surface labelling (**Fig. 5E-G**). We believe this represents nonspecific stickiness as it was
220 indistinguishable to that seen in mock-transfected cells, lacking HTP. The sulfonated first-
221 generation ligand, ATTO 647N-SHTL, substantially reduced this nonspecific intracellular
222 labelling in mock cells (**Fig. 5H-J**), however surface-specific HTP labelling in transfected cells
223 was inefficient, appearing incomplete even at 100 nM; thus, surface labelling could be seen,
224 but with bothersome nonspecific labelling. By contrast, the sulfonated second-generation
225 ATTO 647N-S₂HTL.2 achieved clear labelling when delivered at only 100 nM, revealing bright
226 surface labelling with negligible background (**Fig. 5K**). Even with 1 nM, clean surface labelling
227 was evident after adjusting brightness and contrast (**Fig. 5L, M**). The non-sulfonated ATTO
228 647N-HTL.2 also exhibited efficient labelling (**Fig. S7F-H**), however, nonspecific intracellular
229 was seen if applied at 1000 nM. Thus, by combining HTL.2 with sulfonation, ATTO 647N-
230 S₂HTL.2 performed better than all other ligands tested.

231 The power of chemical biology is often limited by reagent availability. While popular
232 probes are commercially available, variants developed in an academic setting are not always
233 readily available, particularly over longer periods or in larger quantities. We decided to tackle
234 this issue by testing if our one-step protocol to make dye-HTL reagents impermeable can be
235 performed on a small scale without the need for purification, so that any laboratory can perform
236 the synthesis on demand. To facilitate this, we switched the base to sodium *tert*-butoxide,
237 which is soluble to 100 mM in DMSO, making it easier to handle than sodium hydride (**Fig.**
238 **6A**). Neat 1,3-propane sultone was warmed to 35 °C (melting point 32 °C) to obtain a liquid
239 that can straightforwardly be pipetted (**Fig. 6A**). We tested a quick protocol, for which 5 nmol
240 of a dye-HTL is dissolved in 4 μ L of base solution, before addition of 1 μ L of the sultone.
241 Incubation for 5 minutes at room temperature before quenching with 5 μ L PBS yields a 0.5
242 mM dye-SHTL solution that can be directly used for cell application and imaging (**Fig. 6B**). We
243 tested this protocol on commercially available HTL conjugates of JF₅₄₉ and JF₆₄₆, as well as
244 HTL conjugates of our in-house developed probes TMR-d12 and SiR-d12 (**Fig. 6C**). Reactions
245 were >99% quantitative according to LCMS analysis (**Fig. 6D**). It should be noted that the PBS
246 quenching step hydrolyzes the remaining sultone to an impermeable sulfonate, and
247 neutralizes the base. Importantly, we observed no toxicity within 30 minutes of the reaction
248 cocktail when incubating HEK293 cells over 30 min with a 1:1000-dilution (resulting in: [DMSO]

249 = 564 μ M or 0.1%; [sultone] = 108 μ M; [KOtBu] = 4 μ M) tested with a propidium iodide assay
250 for cell death (**Fig. S8**). Furthermore, after exposing HEK293 cells to this cocktail for 24 hours,
251 no effect on cell viability was observed by a WST-1 assay that measures metabolic impact
252 (**Fig. S9**). Higher concentrations led to cell death (LD₅₀ = 2.8 mM DMSO / 535 μ M sultone / 20
253 μ M KOtBu), presumably caused by *tert*-butanol (i.p. LD₅₀ (mouse) = 399 mg/kg), supported
254 by the fact that 14.1 mM DMSO concentrations did not affect viability, and no toxicity reports
255 exist for 3-hydroxypropane-1-sulfonic acid in the National Library of Medicine. Therefore, using
256 a 1:10,000 dilution of the freshly prepared TMR-d12-SHTL (i.e. 50 nM) together with BG-
257 Sulfo646 on HEK293:SNAP-HTP-mGluR2 (both tags on the extracellular side fused to
258 metabotropic glutamate receptor 2) expressing cells (**Fig. 6E**) in confocal imaging, and
259 observed clear co-localization of both channels when using TMR-d12-SHTL and BG-Sulfo646.
260 Similar performance was observed for JF₅₄₉-SHTL, SiR-d12-SHTL, and JF₆₄₆-SHTL (**Fig. 6F**),
261 with the latter showing the cleanest performance.

262 DISCUSSION

263 The development of bright (and impermeable) fluorophores for microscopy has garnered
264 increasing interest,^{11,33,34} particularly in the area of shadow imaging^{35,36} and protein
265 labelling^{7,13,37,38}. In this study, we aimed to install a sulfonate on the amide bond of existing
266 dye-HTL substrates to render them impermeable to a cell's plasma membrane lipid bilayer.
267 This strategy was applied on rhodamine scaffolds, since these dye-HTL molecules only bear
268 one acidic proton, and furthermore, in basic solutions form a non-fluorescent spirolactone
269 form, preventing off-target alkylation on the carboxylate. The majority of dye-HTL reagents
270 should be amenable to this method, however, the approach would not be applicable to certain
271 scaffolds with more possible attachment sites, including biotin, dyes with nucleophilic sites, for
272 instance NH-anilines (e.g. Rho6G, SiR595) or hydroxy groups (e.g. Oregon Green). We
273 observed *cis*- and *trans*-amide mixture in ¹H NMR (see SI), which we were not able to
274 separate, however, we observed full protein labelling by mass spectrometry using recombinant
275 HTP, and observed no difference in labelling kinetics via fluorescence polarization compared
276 to non-sulfonated HTL substrates. We demonstrate impermeability of SHTL conjugates in live
277 cell staining using widefield microscopy on HEK cells transfected with extra- and intracellular
278 localized SNAP and HTP. This allowed live-cell labelling of HTP-mGluR2 transduced
279 hippocampal neurons with SiR-d12-SHTL prior to fixation, antibody staining and confocal
280 imaging. By either specifically targeting the extracellular, exposed HTP-mGluR2 protein pools
281 with SiR-d12-SHTL, or the total protein pool with SiR-d12-HTL, we found that there is a mix of
282 surface and intracellular populations in the soma and both dendritic and axonal processes.
283 Critically, SiR-d12-SHTL allowed us to find the presence of a surface pool of axonal and

284 presynaptically-localized mGluR2. As the trafficking mechanisms and nanolocalization of
285 mGluRs is a highly active field of study,^{20,22,23,39} our observations point towards many surface
286 and intracellular subpopulations of mGluR2, both in the soma and processes/synapses, which
287 will warrant future study, amenable to super-resolution STED nanoscopy. Although we used
288 an overexpression system, our findings open up interesting avenues to probe GPCRs and
289 other receptors in different cellular compartments with precision for surface versus intracellular
290 pools, which we aim to perform on endogenous HTP-fused proteins in the future. For these
291 reasons, we showcase ATTO 647N on the HTL.2 substrate to exhibit cleaner labelling even at
292 low doses down to 1 nM, which may be essential when applied to complex tissues or in live
293 animals, where high concentrations are difficult to achieve. In addition, ATTO 647N has been
294 reported to be sticky, which may lead to nonspecific background labeling,^{40,41} and thus the
295 addition of two negative charges on S₂HTL.2 offers even greater attenuation of nonspecific
296 stickiness. Other dyes that may be interesting, especially due to their performance in the near-
297 infrared, include 2XR-1 (ref⁴²) and heptamethine cyanines⁴³. Finally and generally, a one-step
298 protocol without means of purification for direct application in biology are attractive,^{44,45} and
299 we have added to this portfolio. Although the reaction is near-quantitative, small amounts of
300 starting material left may give rise to intracellular staining (**Fig. S10**). As such, the use of far-
301 red JF₆₄₆-SHTL alongside with 10,000-fold dilutions of the reaction mixture are recommended
302 for surface labelling. We provide a one-page step-by-step protocol for straightforward
303 implementation in the Supporting Information.

304 **SUMMARY**

305 We report on the synthesis and application of sulfonated HaloTag substrates, which can be
306 performed in one step, to label HTP-fused cell surface proteins in the red and far-red.
307 Demonstrated in live cell widefield imaging in HEK293 cells, and in confocal and STED super-
308 resolution microscopy on HTP-mGluR2 transduced hippocampal neurons, we confirm their
309 impermeability and the ability to precisely localize the surface population of a GPCR involved
310 in neurotransmission. We expand the strategy to the second-generation HTL.2, and provide a
311 simple protocol that any laboratory can perform on small scale without the need for purification.
312 While not all substrates are amenable to this approach, we envision wide adoption.

313

314 **AUTHOR CONTRIBUTION**

315 Conceptualization and Methodology: JB; Formal analysis and investigation: KR, SS, CHO,
316 MK, ET, UP, RB, NL and JB; Writing –Original Draft: JL and JB; Reviewing and Editing: KR,
317 JL, NL, ML, MRT, BCS, JH and JB; Visualization: KR and JB; Supervision: NL and JB; Funding
318 Acquisition: JL, NL and JB.

319 **ACKNOWLEDGEMENTS**

320 This project has received funding from the European Union's Horizon Europe Framework
321 Programme (deuterON, grant agreement no. 101042046 to JB). This work was supported by
322 the German Research Foundation Excellence Strategy EXC-2049-390688087 (NL) and CRC
323 1286 "Quantitative Synaptology" project A11 (NL). HTL.2 reagents were supported by NIH
324 grants 1RF1MH117055 and 1DP2MH1194025 (to MRT). JL is supported by NIH grant
325 R01NS129904.

326 **COMPETING INTERESTS**

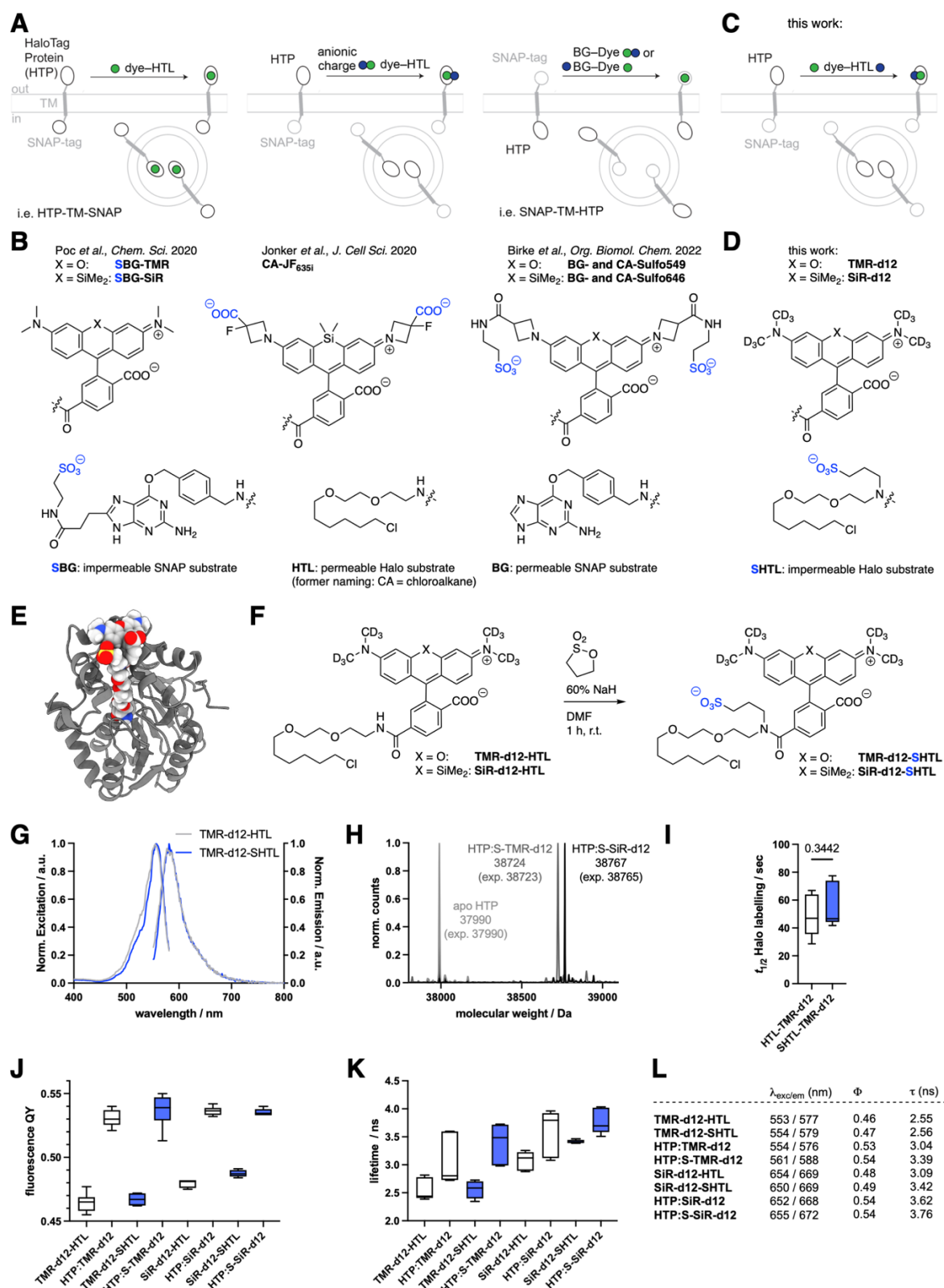
327 NL is a member of the scientific advisory board of Trace Neuroscience. MRT and BCS are on
328 patent applications describing HTL.2. All other authors declare no competing interests.

329 **MATERIALS AND METHODS**

330 Chemical synthesis and characterization, modelling, measurements of photophysical and
331 kinetic parameters, and procedures in cell culture, molecular biology and imaging are reported
332 in the Supporting Information.

333

334 **FIGURES**

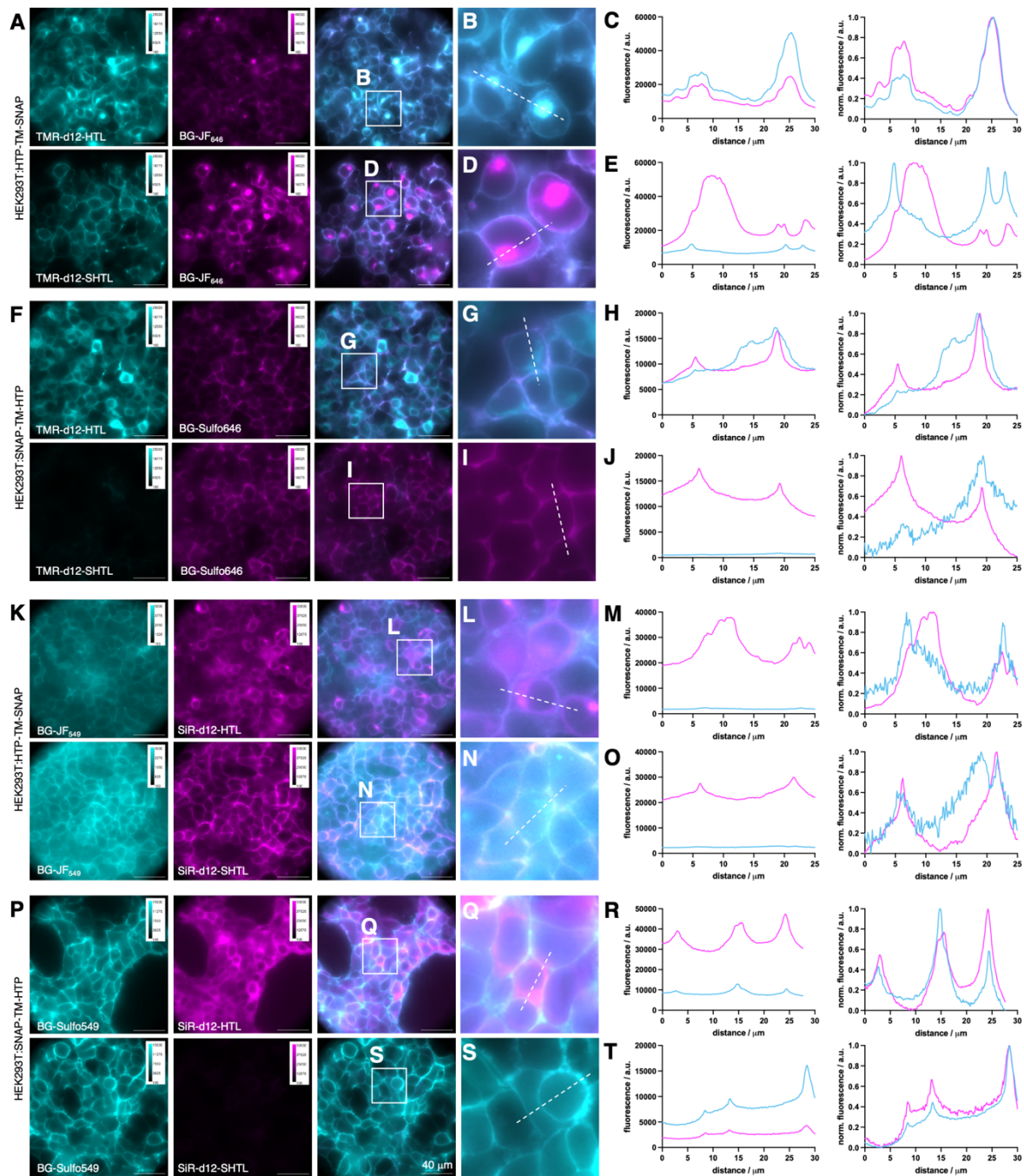


335

336 **Figure 1: Logic for impermeable dyes to label cell surface proteins. A-B)** Known
 337 strategies to address extracellularly exposed self-labelling tags with cartoons and chemical
 338 structures indicating where anionic charges have previously been introduced. **C-D)** Our new
 339 strategy to install a sulfonate charge on the HaloTag Ligand (HTL). **E)** Modelling of the HaloTag

340 Protein (HTP) bound to TMR-SHTL. **F)** Synthesis of TMR-d12-SHTL and SiR-d12-SHTL. **G)**
341 Excitation and emission profiles of TMR-d12 comparing HTL to SHTL conjugates. **H)** *In vitro*
342 protein labelling of apo-HTP confirms binding by full protein mass spectrometry. **I)** Labelling
343 kinetics of apo-HTP with TMR-d12-HTL and TMR-d12-SHTL. **J)** Fluorescence quantum yields
344 of TMR/SiR-d12 conjugated to HTL/SHTL with or without HTP-bound. **K)** Fluorescence
345 lifetimes of the same reagents. **L)** Table summarizing values from G, J, K.

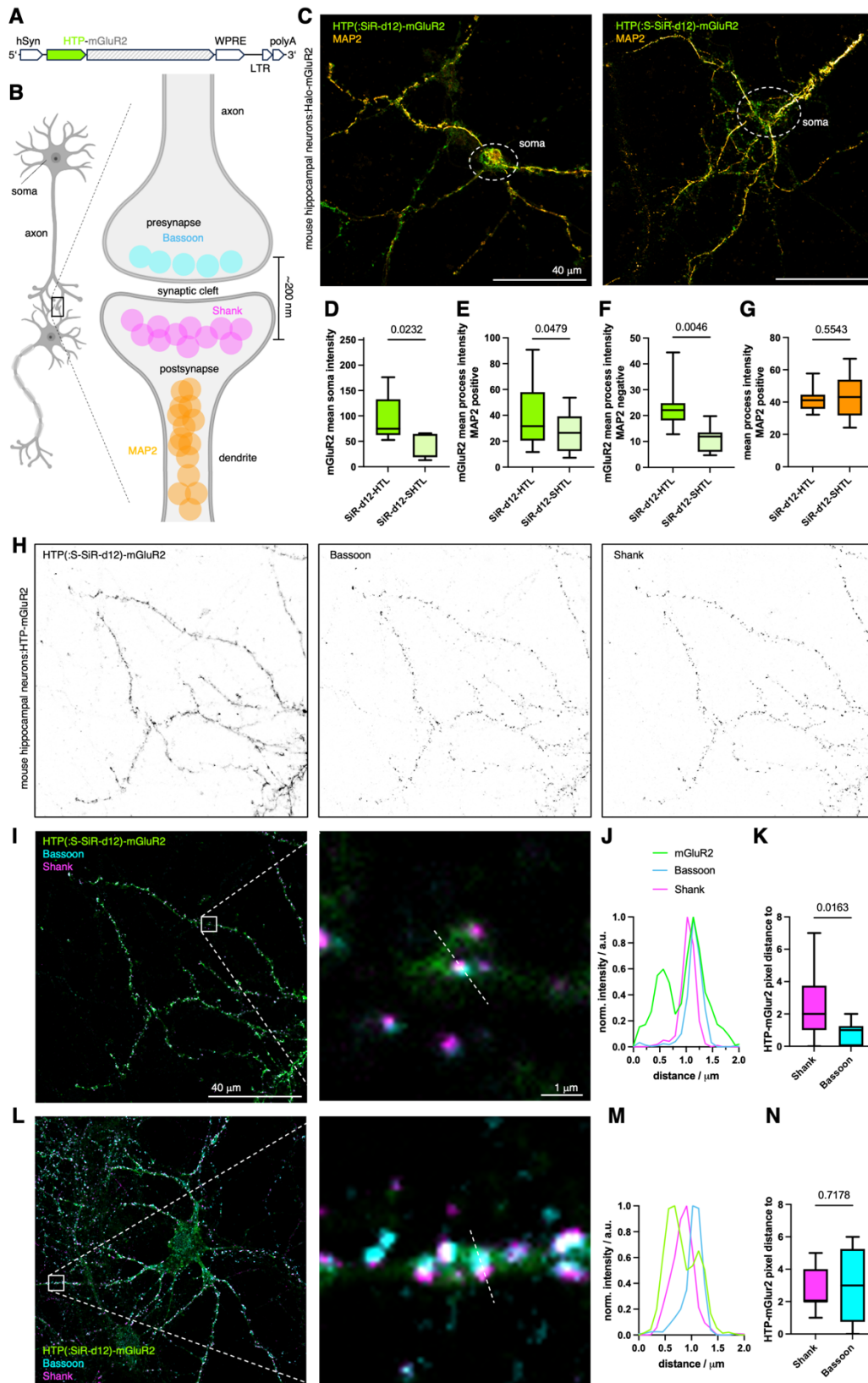
346



347

348 **Figure 2: Live cell imaging in transfected HE293 cells. A-E)** HEK293 expressing HTP-TM-
 349 SNAP. Intracellular SNAP labelled with BG-JF₆₄₆; extracellular HTP labelled with TMR-d12-
 350 HTL or TMR-d12-SHTL. Widefield imaging (A), zoom-ins (B, D) and line scans (C, E). **F-J)**
 351 HEK293 cells expressing SNAP-TM-HTP. Extracellular SNAP labelled with BG-SulfoJF₆₄₆;
 352 intracellular HTP labelled with TMR-d12-HTL or TMR-d12-SHTL. Widefield (F), zoom-in (G, I)
 353 and line scans (H, J). **K-O)** As for A-E but staining with BG-JF₅₄₉ and SiR-d12-(S)HTL . **P-T)**
 354 As for F-J but staining with BG-SulfoJF₅₄₉ and SiR-d12-(S)HTL.

355

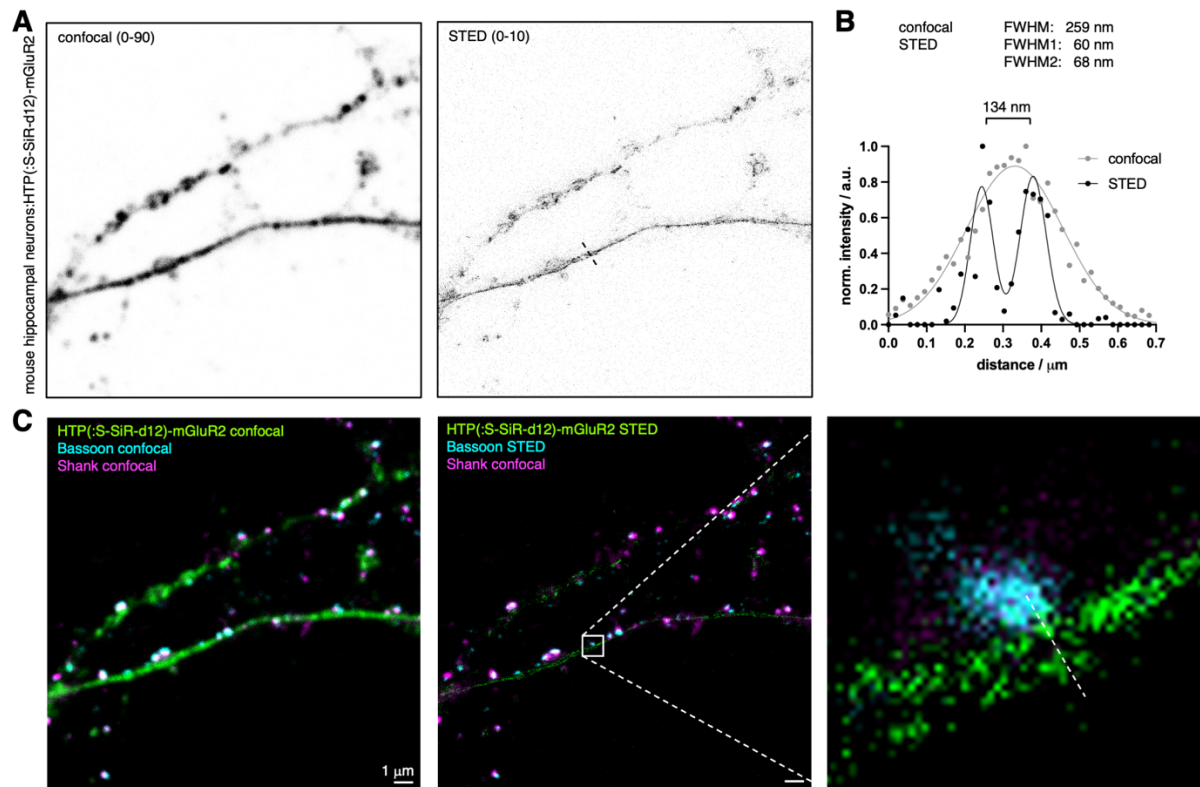


356

357 **Figure 3: Revealing HTP-mGluR2 localization in hippocampal neurons.** **A)** Viral DNA
 358 expression cassette with HTP-mGluR under hSyn promoter. **B)** Neural connection via
 359 synapses and localization of axonal MAP2, presynaptic Bassoon and postsynaptic Shank
 360 proteins (created in biorender.com). **C)** Confocal imaging of HTP-mGluR2 transduced mouse
 361 hippocampal neurons with SiR-d12-SHTL (left) and SiR-d12-HTL (right), co-stained with an

362 antibody against MAP2 for dendrite identification. **D-G)** Quantification of HTP-mGluR2
363 labelling in the soma (D), in dendrites (MAP2 positive, E) and in axons (MAP2 negative, F)
364 reveals significantly less signal using SiR-d12-SHTL, while no difference in axonal MAP2
365 intensity is observed (G). Mean±SD. Student's t-test. **H)** Confocal imaging of HTP-mGluR2
366 transduced mouse hippocampal neurons cells with SiR-d12-SHTL (500 nM), and the pre- and
367 postsynaptic markers Bassoon and Shank, respectively. **I)** Overlay of images in H. **J)**
368 Representative line scan of a synapse shows mGluR2 co-localization primarily with the
369 presynaptic marker Bassoon. **K)** Quantification of mGluR2 localization with respect to
370 Bassoon and Shank. Mean±SD. Student's t-test. **L-M)** As for I-K but labelling with SiR-d12-
371 HTL.

372

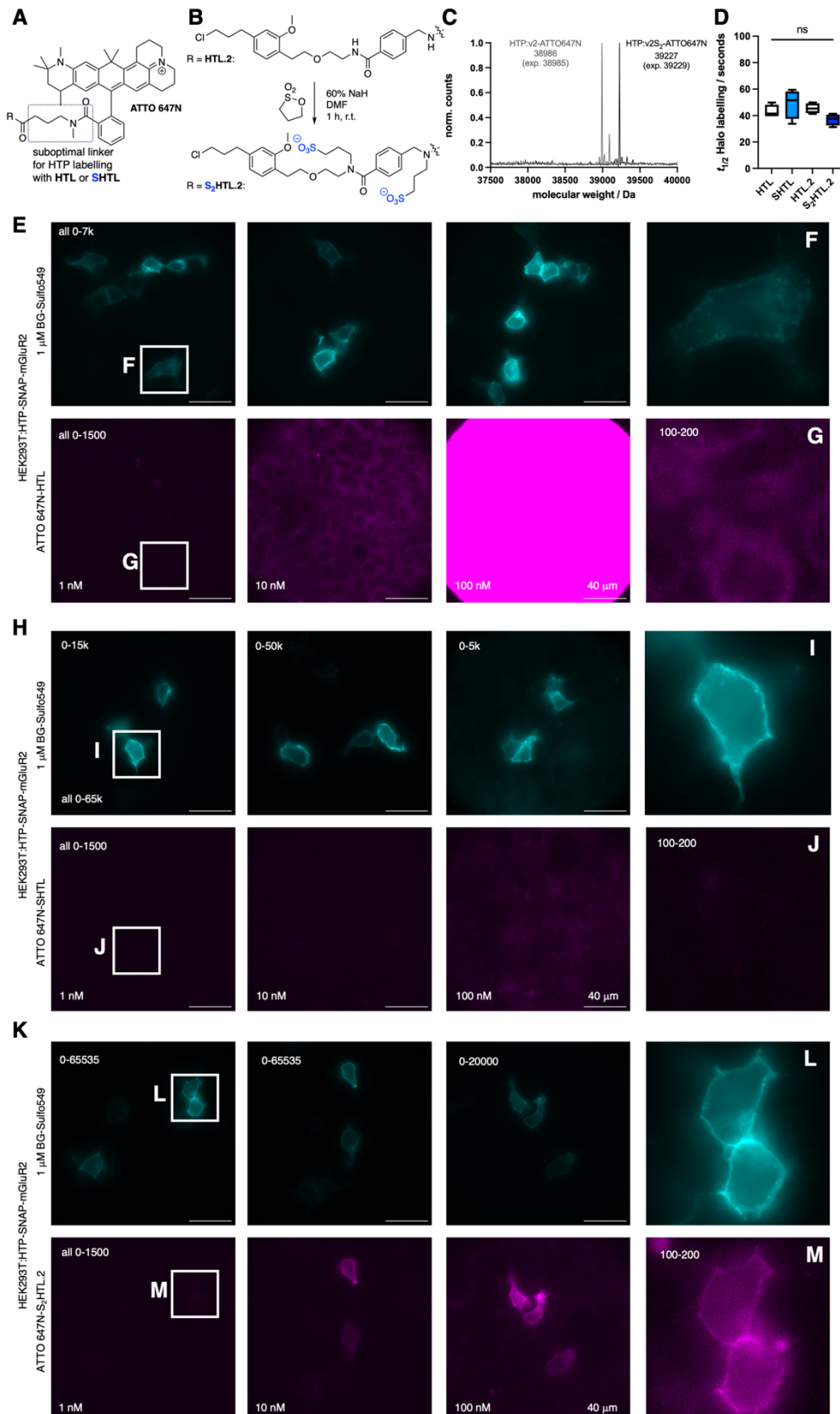


373

374 **Figure 4: STED super-resolution imaging of surface HTP(:S-SiR-d12)-mGluR2. A)**
375 **Confocal and STED images of HTP(:S-SiR-d12)-mGluR2 transduced neurons. B)** Line scan
376 **profile of a process comparing confocal to STED performance, yielding a resolution of 134 nm**
377 **across the ultrastructure. C) Confocal and dual color STED with zoom in of the process**
378 **reported in (B).**

379

380



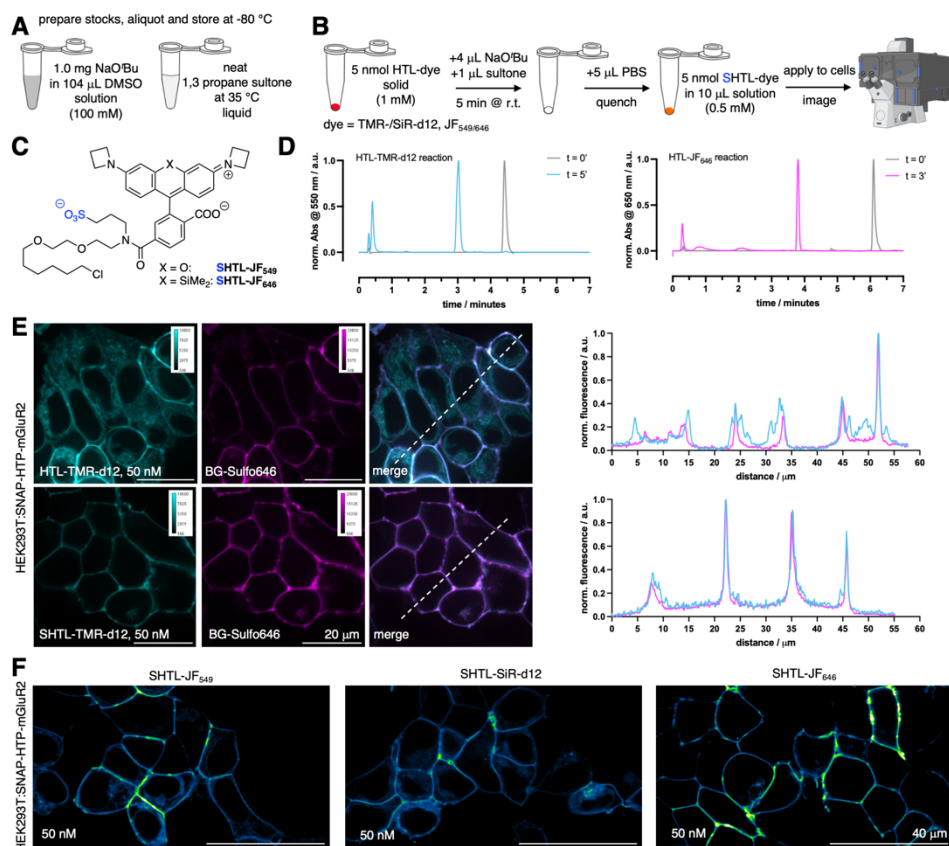
381

382 **Figure 5: Sulfonation on the HaloTag ligand v2.0 (HTL.2) for improved labelling with**
 383 **sticky ATTO 647N. A) Chemical structure of ATTO 647N, with a *N*-methyl amidated additional**
 384 **four carbon linker on the 3 position, which disallows proper dye:HTP secondary interactions.**

385 **B)** Sulfonation protocol on second version HaloTag ligand HTL.2 yields double sulfonated
386 S₂HTL.2. **C)** qTOF full protein mass spectrometry of recombinant HTP labelled with ATTO
387 647N-HTL.2 and ATTO 647N-S₂HTL.2. **E)** HTP-SNAP- mGluR2 transfected HEK293 cells,
388 labelled with BG-Sulfo549 (1 uM) and different concentrations of ATTO 647N-HTL.2 for 10
389 minutes prior to fixation and imaging gives rise to unspecific signal. **F, G)** Zoom ins and
390 brightness contrast adjusted images from (E). **H-J)** As for (E-G) but with different
391 concentrations of ATTO 647N-SHTL leads to image improvements by removing unspecific
392 signals. **K-M)** As for (E-G) but with different concentrations of ATTO 647N-S₂HTL.2 allows
393 clear membrane labelling even at 1 nM.

394

395



396

397 **Figure 6: One step protocol on small scale to synthesize and apply dye-SHTL. A)**
 398 Required stock solutions. **B)** Outlined 5-minute synthetic protocol (partly created in
 399 biorender.com). **C)** Structures of JF_{549/646}-SHTL. **D)** LCMS traces of the reaction for TMR-
 400 d12-HTL and JF₆₄₆-HTL. **E)** Confocal imaging of HEK293:SNAP-HTP-mGluR2 transfected
 401 cells with TMR-d12-(S)HTL (50 nM) and BG-Sulfo646 (50 nM) including line scans. **F)** As for
 402 E, but with JF₅₄₉-SHTL, SiR-d12-SHTL and JF₆₄₆-SHTL.

403

404 REFERENCES

- 405 1. Bosch, P.J., Corrêa, I.R., Sonntag, M.H., Ibach, J., Brunsveld, L., Kanger, J.S., and
406 Subramaniam, V. (2014). Evaluation of Fluorophores to Label SNAP-Tag Fused Proteins
407 for Multicolor Single-Molecule Tracking Microscopy in Live Cells. *Biophysical Journal* 107,
408 803–814. <https://doi.org/10.1016/j.bpj.2014.06.040>.
- 409 2. Erdmann, R.S., Baguley, S.W., Richens, J.H., Wissner, R.F., Xi, Z., Allgeyer, E.S., Zhong,
410 S., Thompson, A.D., Lowe, N., Butler, R., et al. (2019). Labeling Strategies Matter for
411 Super-Resolution Microscopy: A Comparison between HaloTags and SNAP-tags. *Cell*
412 *Chemical Biology* 26, 584-592.e6. <https://doi.org/10.1016/j.chembiol.2019.01.003>.
- 413 3. Cook, A., Walterspiel, F., and Deo, C. (2023). HaloTag-Based Reporters for Fluorescence
414 Imaging and Biosensing. *ChemBioChem* 24, e202300022.
415 <https://doi.org/10.1002/cbic.202300022>.
- 416 4. Los, G.V., Encell, L.P., McDougall, M.G., Hartzell, D.D., Karassina, N., Zimprich, C.,
417 Wood, M.G., Learish, R., Ohana, R.F., Urh, M., et al. (2008). HaloTag: A Novel Protein
418 Labeling Technology for Cell Imaging and Protein Analysis. *ACS Chem. Biol.* 3, 373–382.
419 <https://doi.org/10.1021/cb800025k>.
- 420 5. England, C.G., Luo, H., and Cai, W. (2015). HaloTag Technology: A Versatile Platform for
421 Biomedical Applications. *Bioconjugate Chem.* 26, 975–986.
422 <https://doi.org/10.1021/acs.bioconjchem.5b00191>.
- 423 6. Jonker, C.T.H., Deo, C., Zager, P.J., Tkachuk, A.N., Weinstein, A.M., Rodriguez-Boulan,
424 E., Lavis, L.D., and Schreiner, R. (2019). Accurate measurement of fast endocytic
425 recycling kinetics in real time. *J Cell Sci.* <https://doi.org/10.1242/jcs.231225>.
- 426 7. Birke, R., Ast, J., Roosen, D.A., Lee, J., Roßmann, K., Huhn, C., Mathes, B., Lisurek, M.,
427 Bushiri, D., Sun, H., et al. (2022). Sulfonated red and far-red rhodamines to visualize
428 SNAP- and Halo-tagged cell surface proteins. *Org Biomol Chem* 20, 5967–5980.
429 <https://doi.org/10.1039/d1ob02216d>.
- 430 8. Grimm, J.B., English, B.P., Chen, J., Slaughter, J.P., Zhang, Z., Revyakin, A., Patel, R.,
431 Macklin, J.J., Normanno, D., Singer, R.H., et al. (2015). A general method to improve
432 fluorophores for live-cell and single-molecule microscopy. *Nat. Methods* 12, 244–250.
433 <https://doi.org/10.1038/nmeth.3256>.
- 434 9. Wang, L., Tran, M., D'Este, E., Roberti, J., Koch, B., Xue, L., and Johnsson, K. (2019). A
435 general strategy to develop cell permeable and fluorogenic probes for multicolour
436 nanoscopy. *Nat. Chem.*, 1–8. <https://doi.org/10.1038/s41557-019-0371-1>.
- 437 10. Eiring, P., McLaughlin, R., Matikonda, S.S., Han, Z., Grabenhorst, L., Helmerich, D.A.,
438 Meub, M., Beliu, G., Luciano, M., Bandi, V., et al. (2021). Targetable Conformationally
439 Restricted Cyanines Enable Photon-Count-Limited Applications**. *Angew Chem Int Ed* 60,
440 26685–26693. <https://doi.org/10.1002/anie.202109749>.
- 441 11. Schnermann, M.J., and Lavis, L.D. (2023). Rejuvenating old fluorophores with new
442 chemistry. *Current Opinion in Chemical Biology* 75, 102335.
443 <https://doi.org/10.1016/j.cbpa.2023.102335>.
- 444 12. Selvakumar, P., Lee, J., Khanra, N., He, C., Munguba, H., Kiese, L., Broichhagen, J.,
445 Reiner, A., Levitz, J., and Meyerson, J.R. (2021). Structural and compositional diversity in

- 446 the kainate receptor family. *Cell Rep.* 37, 109891.
447 <https://doi.org/10.1016/j.celrep.2021.109891>.
- 448 13. Lee, J., Gonzalez-Hernandez, A.J., Kristt, M., Abreu, N., Roßmann, K., Arefin, A., Marx,
449 D.C., Broichhagen, J., and Levitz, J. (2023). Distinct beta-arrestin coupling and
450 intracellular trafficking of metabotropic glutamate receptor homo- and heterodimers. *Sci.*
451 *Adv.* 9, eadi8076. <https://doi.org/10.1126/sciadv.adi8076>.
- 452 14. Poc, P., Gutzeit, V.A., Ast, J., Lee, J., Jones, B.J., D'Este, E., Mathes, B., Lehmann, M.,
453 Hodson, D.J., Levitz, J., et al. (2020). Interrogating surface *versus* intracellular
454 transmembrane receptor populations using cell-impermeable SNAP-tag substrates.
455 *Chem. Sci.* 11, 7871–7883. <https://doi.org/10.1039/D0SC02794D>.
- 456 15. Bianco, G., Forli, S., Goodsell, D.S., and Olson, A.J. (2016). Covalent docking using
457 autodock: Two-point attractor and flexible side chain methods. *Protein Science* 25, 295–
458 301. <https://doi.org/10.1002/pro.2733>.
- 459 16. Morris, G.M., Huey, R., Lindstrom, W., Sanner, M.F., Belew, R.K., Goodsell, D.S., and
460 Olson, A.J. (2009). AutoDock4 and AutoDockTools4: Automated docking with selective
461 receptor flexibility. *J Comput Chem* 30, 2785–2791. <https://doi.org/10.1002/jcc.21256>.
- 462 17. Wilhelm, J., Kühn, S., Tarnawski, M., Gotthard, G., Tünnermann, J., Tänzer, T.,
463 Karpenko, J., Mertes, N., Xue, L., Uhrig, U., et al. (2021). Kinetic and Structural
464 Characterization of the Self-Labeling Protein Tags HaloTag7, SNAP-tag, and CLIP-tag.
465 *Biochemistry* 60, 2560–2575. <https://doi.org/10.1021/acs.biochem.1c00258>.
- 466 18. Roßmann, K., Akkaya, K.C., Poc, P., Charbonnier, C., Eichhorst, J., Gonschior, H.,
467 Valavalkar, A., Wendler, N., Cordes, T., Dietzek-Ivanšić, B., et al. (2022). N-Methyl
468 deuterated rhodamines for protein labelling in sensitive fluorescence microscopy. *Chem*
469 *Sci* 13, 8605–8617. <https://doi.org/10.1039/d1sc06466e>.
- 470 19. Acosta-Ruiz, A., Gutzeit, V.A., Skelly, M.J., Meadows, S., Lee, J., Parekh, P., Orr, A.G.,
471 Liston, C., Pleil, K.E., Broichhagen, J., et al. (2020). Branched Photoswitchable Tethered
472 Ligands Enable Ultra-efficient Optical Control and Detection of G Protein-Coupled
473 Receptors In Vivo. *Neuron* 105, 446–463.e13.
474 <https://doi.org/10.1016/j.neuron.2019.10.036>.
- 475 20. Reiner, A., and Levitz, J. (2018). Glutamatergic Signaling in the Central Nervous System:
476 Ionotropic and Metabotropic Receptors in Concert. *Neuron* 98, 1080–1098.
477 <https://doi.org/10.1016/j.neuron.2018.05.018>.
- 478 21. Jin, L.E., Wang, M., Galvin, V.C., Lightbourne, T.C., Conn, P.J., Arnsten, A.F.T., and
479 Paspalas, C.D. (2018). mGluR2 versus mGluR3 Metabotropic Glutamate Receptors in
480 Primate Dorsolateral Prefrontal Cortex: Postsynaptic mGluR3 Strengthen Working
481 Memory Networks. *Cerebral Cortex* 28, 974–987. <https://doi.org/10.1093/cercor/bhx005>.
- 482 22. Bodzęta, A., Scheefhals, N., and MacGillavry, H.D. (2021). Membrane trafficking and
483 positioning of mGluRs at presynaptic and postsynaptic sites of excitatory synapses.
484 *Neuropharmacology* 200, 108799. <https://doi.org/10.1016/j.neuropharm.2021.108799>.
- 485 23. Bodzęta, A., Berger, F., and MacGillavry, H.D. (2022). Subsynaptic mobility of
486 presynaptic mGluR types is differentially regulated by intra- and extracellular interactions.
487 *MBoC* 33, ar66. <https://doi.org/10.1091/mbc.E21-10-0484>.

- 488 24. Meyer, S.A., Ozbay, B.N., Potcoava, M., Salcedo, E., Restrepo, D., and Gibson, E.A.
489 (2016). Super-resolution imaging of ciliary microdomains in isolated olfactory sensory
490 neurons using a custom two-color stimulated emission depletion microscope. *J. Biomed.*
491 *Opt* 21, 066017. <https://doi.org/10.1117/1.JBO.21.6.066017>.
- 492 25. Gonzalez Pisfil, M., Nadelson, I., Bergner, B., Rottmeier, S., Thomae, A.W., and Dietzel,
493 S. (2022). Stimulated emission depletion microscopy with a single depletion laser using
494 five fluorochromes and fluorescence lifetime phasor separation. *Sci Rep* 12, 14027.
495 <https://doi.org/10.1038/s41598-022-17825-5>.
- 496 26. Han, Y., Li, M., Qiu, F., Zhang, M., and Zhang, Y.-H. (2017). Cell-permeable organic
497 fluorescent probes for live-cell long-term super-resolution imaging reveal lysosome-
498 mitochondrion interactions. *Nat Commun* 8, 1307. <https://doi.org/10.1038/s41467-017-01503-6>.
- 500 27. Liu, W., Liu, Q., Zhang, Z., Han, Y., Kuang, C., Xu, L., Yang, H., and Liu, X. (2019).
501 Three-dimensional super-resolution imaging of live whole cells using galvanometer-based
502 structured illumination microscopy. *Opt. Express* 27, 7237.
503 <https://doi.org/10.1364/OE.27.007237>.
- 504 28. Meissner, G.W., Grimm, J.B., Johnston, R.M., Sutcliffe, B., Ng, J., Jefferis, G.S.X.E.,
505 Cachero, S., Lavis, L.D., and Malkesman, O. (2018). Optimization of fluorophores for
506 chemical tagging and immunohistochemistry of *Drosophila* neurons. *PLoS ONE* 13,
507 e0200759. <https://doi.org/10.1371/journal.pone.0200759>.
- 508 29. Kolmakov, K., Hebisch, E., Wolfram, T., Nordwig, L.A., Wurm, C.A., Ta, H., Westphal, V.,
509 Belov, V.N., and Hell, S.W. (2015). Far-Red Emitting Fluorescent Dyes for Optical
510 Nanoscopy: Fluorinated Silicon–Rhodamines (SiRF Dyes) and Phosphorylated Oxazines.
511 *Chemistry A European J* 21, 13344–13356. <https://doi.org/10.1002/chem.201501394>.
- 512 30. Wilhelm, J., Kühn, S., Tarnawski, M., Gotthard, G., Tünnermann, J., Tänzler, T.,
513 Karpenko, J., Mertes, N., Xue, L., Uhrig, U., et al. (2021). Kinetic and Structural
514 Characterization of the Self-Labeling Protein Tags HaloTag7, SNAP-tag, and CLIP-tag.
515 *Biochemistry* 60, 2560–2575. <https://doi.org/10.1021/acs.biochem.1c00258>.
- 516 31. Shields, B.C., Yan, H., Lim, S.S.X., Burwell, S.C.V., Cammarata, C.M., Fleming, E.A.,
517 Yousefzadeh, S.A., Goldenshtein, V.Z., Kahuno, E.W., Vagadia, P.P., et al. (2024).
518 DART.2: bidirectional synaptic pharmacology with thousandfold cellular specificity. *Nat*
519 *Methods* 21, 1288–1297. <https://doi.org/10.1038/s41592-024-02292-9>.
- 520 32. Shields, B.C., Kahuno, E., Kim, C., Apostolides, P.F., Brown, J., Lindo, S., Mensh, B.D.,
521 Dudman, J.T., Lavis, L.D., and Tadross, M.R. (2017). Deconstructing behavioral
522 neuropharmacology with cellular specificity. *Science* 356, eaaj2161.
523 <https://doi.org/10.1126/science.aaj2161>.
- 524 33. Jiang, G., Liu, H., Liu, H., Ke, G., Ren, T., Xiong, B., Zhang, X., and Yuan, L. (2024).
525 Chemical Approaches to Optimize the Properties of Organic Fluorophores for Imaging
526 and Sensing. *Angew Chem Int Ed* 63, e202315217.
527 <https://doi.org/10.1002/anie.202315217>.
- 528 34. Munan, S., Chang, Y.-T., and Samanta, A. (2024). Chronological development of
529 functional fluorophores for bio-imaging. *Chem. Commun.* 60, 501–521.
530 <https://doi.org/10.1039/D3CC04895K>.

- 531 35. Tønnesen, J., Inavalli, V.V.G.K., and Nägerl, U.V. (2018). Super-Resolution Imaging of
532 the Extracellular Space in Living Brain Tissue. *Cell* 172, 1108-1121.e15.
533 <https://doi.org/10.1016/j.cell.2018.02.007>.
- 534 36. Velicky, P., Miguel, E., Michalska, J.M., Lyudchik, J., Wei, D., Lin, Z., Watson, J.F., Troidl,
535 J., Beyer, J., Ben-Simon, Y., et al. (2023). Dense 4D nanoscale reconstruction of living
536 brain tissue. *Nat Methods* 20, 1256–1265. <https://doi.org/10.1038/s41592-023-01936-6>.
- 537 37. Calebiro, D., Rieken, F., Wagner, J., Sungkaworn, T., Zabel, U., Borzi, A., Cocucci, E.,
538 Zürn, A., and Lohse, M.J. (2013). Single-molecule analysis of fluorescently labeled G-
539 protein-coupled receptors reveals complexes with distinct dynamics and organization.
540 *Proc. Natl. Acad. Sci. U.S.A.* 110, 743–748. <https://doi.org/10.1073/pnas.1205798110>.
- 541 38. Ast, J., Nasteska, D., Fine, N.H.F., Nieves, D.J., Koszegi, Z., Lanoiselée, Y., Cuozzo, F.,
542 Vioria, K., Bacon, A., Luu, N.T., et al. (2023). Revealing the tissue-level complexity of
543 endogenous glucagon-like peptide-1 receptor expression and signaling. *Nat Commun* 14,
544 301. <https://doi.org/10.1038/s41467-022-35716-1>.
- 545 39. Siddig, S., Aufmkolk, S., Doose, S., Jobin, M.-L., Werner, C., Sauer, M., and Calebiro, D.
546 (2020). Super-resolution imaging reveals the nanoscale organization of metabotropic
547 glutamate receptors at presynaptic active zones. *Sci. Adv.* 6, eaay7193.
548 <https://doi.org/10.1126/sciadv.aay7193>.
- 549 40. Yao, J.Z., Uttamapinant, C., Poloukhtine, A., Baskin, J.M., Codelli, J.A., Sletten, E.M.,
550 Bertozzi, C.R., Popik, V.V., and Ting, A.Y. (2012). Fluorophore Targeting to Cellular
551 Proteins via Enzyme-Mediated Azide Ligation and Strain-Promoted Cycloaddition. *J. Am.*
552 *Chem. Soc.* 134, 3720–3728. <https://doi.org/10.1021/ja208090p>.
- 553 41. Zanetti-Domingues, L.C., Tynan, C.J., Rolfe, D.J., Clarke, D.T., and Martin-Fernandez,
554 M. (2013). Hydrophobic Fluorescent Probes Introduce Artifacts into Single Molecule
555 Tracking Experiments Due to Non-Specific Binding. *PLoS ONE* 8, e74200.
556 <https://doi.org/10.1371/journal.pone.0074200>.
- 557 42. Wu, W., Yan, K., He, Z., Zhang, L., Dong, Y., Wu, B., Liu, H., Wang, S., and Zhang, F.
558 (2024). 2X-Rhodamine: A Bright and Fluorogenic Scaffold for Developing Near-Infrared
559 Chemigenetic Indicators. *J Am Chem Soc.* <https://doi.org/10.1021/jacs.4c03485>.
- 560 43. Janeková, H., Friedman, H.C., Russo, M., Zyberaj, M., Ahmed, T., Hua, A.S., Sica, A.V.,
561 Caram, J.R., and Štacko, P. (2024). Deuteration of heptamethine cyanine dyes enhances
562 their emission efficacy. *Chem. Commun.* 60, 1000–1003.
563 <https://doi.org/10.1039/D3CC05153F>.
- 564 44. Cabré, G., Garrido-Charles, A., Moreno, M., Bosch, M., Porta-de-la-Riva, M., Krieg, M.,
565 Gascón-Moya, M., Camarero, N., Gelabert, R., Lluch, J.M., et al. (2019). Rationally
566 designed azobenzene photoswitches for efficient two-photon neuronal excitation. *Nat*
567 *Commun* 10, 907. <https://doi.org/10.1038/s41467-019-08796-9>.
- 568 45. Thomas, R.P., Heap, R.E., Zappacosta, F., Grant, E.K., Pogány, P., Besley, S., Fallon,
569 D.J., Hann, M.M., House, D., Tomkinson, N.C.O., et al. (2021). A direct-to-biology high-
570 throughput chemistry approach to reactive fragment screening. *Chem. Sci.* 12, 12098–
571 12106. <https://doi.org/10.1039/D1SC03551G>.

572